Removal of water-vapor-induced fluctuations in T-ray signals: A preliminary study

W. Withayachumnankul, B. M. Fischer, S. P. Mickan, and D. Abbott

Centre for Biomedical Engineering and School of Electrical & Electronic Engineering,
The University of Adelaide Adelaide, SA 5005, Australia

ABSTRACT

In an open-air setting, one source of fluctuations in a T-ray (THz) pulsed signal is attributed to water vapor. Fluctuations of this type are generally undesired, and so the water vapor is commonly removed in a closed chamber. Yet, in some applications a closed chamber is not feasible. This paper presents a preliminary study on a computational means to address the problem. Initially, the complex frequency response of water vapor is modeled from spectral line data. Using a deconvolution technique, together with fine tuning of the line strength at each frequency, the response is partially removed from a measured T-ray pulse, with minimal signal distortion.

Keywords: THz-TDS, T-rays, terahertz, absorption line, water-vapor-induced fluctuations, femtosecond laser systems, fluctuation ratio

1. INTRODUCTION

Terahertz time-domain spectroscopy (THz-TDS) has received much attention from researchers due to its outstanding performance.[1] With the assistance of ultrafast femtosecond laser technology, a T-ray emitter can radiate a short pulse, the frequencies of which span from a few hundred gigahertz to a few terahertz or more. This frequency range has a high black-body radiation background, prohibiting a high-SNR detection with a conventional detector. However, this problem can be suppressed by adopting a coherent detection scheme, lifting the SNR to as high as 60 dB.[2]

A number of molecules of general interest have unique rotational[3] and vibrational[4] transition energies in the T-ray frequency band. Because of these unique fingerprints, THz-TDS is useful for material classification and recognition. However, this property, on the other hand, affects the THz-TDS capability in an open air setting, in which water vapor is ubiquitous.

Essentially, liquid water highly absorbs T-rays, due to intermolecular interactions.[5] Water vapor residue in a T-ray propagation path gives rise to many rotational absorption lines in a T-ray spectrum.[6] Spectroscopy of a material, in open air, therefore results in a combination of the material's spectral features and water absorption lines in the frequency domain. In the time domain, this results in field fluctuation after the main T-ray pulse. Mostly, these effects are undesirable, since they can obscure a meaningful spectroscopic result.

The water-vapor effects are removable during the measurement stage by purging an enclosed T-ray path with dry air or a non-polar gas such as nitrogen,[7] which does not have transition energy levels in the T-ray regime. In some applications, it is not always possible to cover the entire T-ray beam path with dry atmosphere, for example in the applications where stand-off detection is required.[8] In such cases, performing narrowband T-ray sensing in an atmospheric transmission window could avoid the effects,[9] at the expense of a full spectral fingerprint. A numerical method to circumvent the water vapor effects would therefore be beneficial.

Knowing the absorption lines' positions and strengths in the T-ray frequency range allows numerical estimation of the complex response of water vapor. Theoretically, the vapor complex response can be deconvolved directly from a received T-ray signal. This can be achieved without affecting the main pulse, reflections (if any), and other unrelated features, depending on the sample under measurement. But, in fact, the modeled complex response of water vapor does not exactly fit to the measured response, due to measurement uncertainties,[10]

Email addresses: withawat@eleceng.adelaide.edu.au (W. Withayachumnankul); spmickan@eleceng.adelaide.edu.au (S. P. Mickan); bfischer@eleceng.adelaide.edu.au (B. M. Fischer); dabbott@eleceng.adelaide.edu.au (D. Abbott)

Noise and Fluctuations in Photonics, Quantum Optics, and Communications
edited by Leon Cohen, Proc. of SPIE Vol. 6603, 660323, (2007)
0277-786X/07/$18 · doi: 10.1117/12.724616

limited dynamic range[11] and limited frequency resolution[12] of the system, etc.—among these factors, the limited dynamic range causes significant discrepancy. Since the dynamic range sets the maximum absorption that the system can measure, any absorption line that has strength beyond this limit will be clipped in magnitude.

Fine-tuning the strength of a complex absorption line based on a brute-force search is introduced in this paper. Each absorption line is tuned in magnitude within a predefined range and then deconvolved from the measured signal. A criterion is met when the ratio of the main pulse energy to the fluctuation energy of the adjusted signal is maximized. Repeatedly tuning the strength line-by-line ultimately results in the mitigation of water-vapor-induced fluctuations.

The proposed algorithm has merits in that (i) its generality allows application to T-ray signals with less effect on samples' temporal and spectral features, and (ii) the exact atmospheric conditions, including humidity, temperature, and propagation length, are not crucial in order to remove the water-vapor response.

This paper is organized as follows: Section 2 gives basic insight into a THz-TDS system. Section 3 elaborates the effects of water vapor on T-ray signals and spectra. Section 4 considers the entire measurement as a system with several complex responses, and suggests the possibility of removing water-vapor response. Section 5 models the complex response of water vapor, and emphasizes the discrepancy between the model and measurement. In Section 6, a fine-tuning algorithm to overcome the discrepancy issue is devised, and fluctuation ratio is proposed as a measure of tuning. This algorithm is tested in Section 7, followed by discussions and a conclusion in Section 8.

2. THZ-TDS SYSTEM

The THz-TDS system shown in Figure 1 is mainly composed of an ultrafast optical laser, T-ray emitter/receiver, an optical delay line, a set of mirrors, a material sample, and a chamber. The ultrafast optical pulse is divided into two paths, a probe beam and a pump beam, by a beam splitter. At the emitter, the optical pump beam stimulates T-ray pulsed radiation via either charge transport[13] or optical rectification effect,[14] depending on the emitter type. The diverging T-ray beam is collimated and focuses onto the sample by a lenses and a pair of parabolic mirrors. After passing through the sample, the T-ray beam is re-collimated and focused onto the

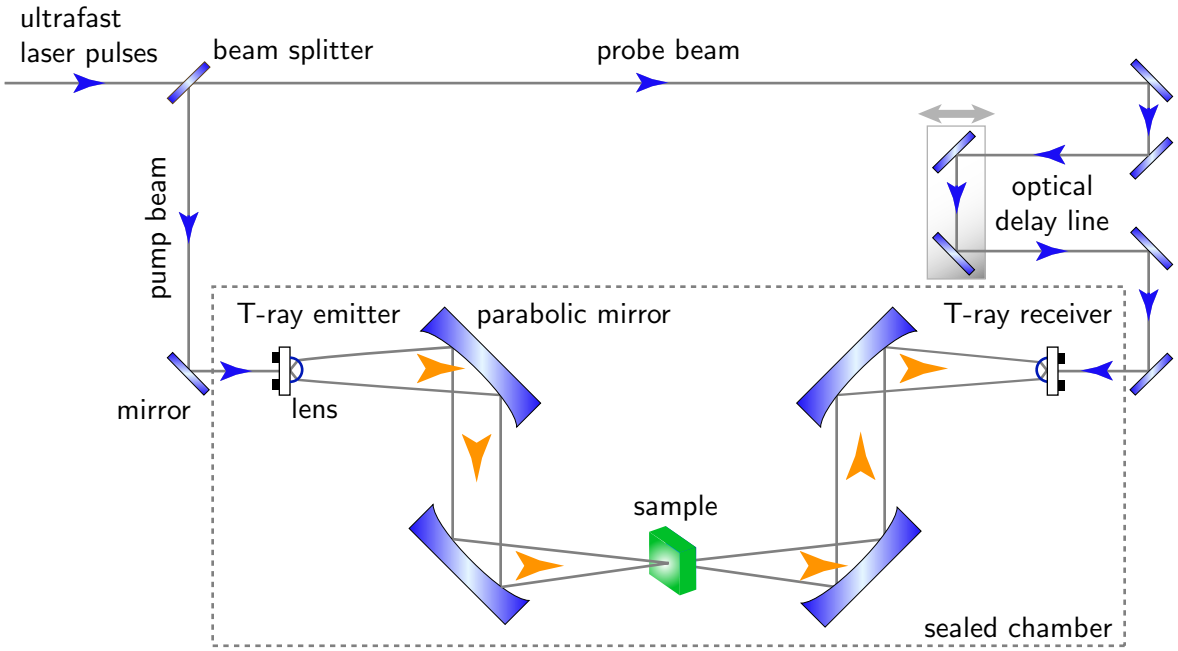

Figure 1. THz-TDS system configured in transmission mode with PCA generation and detection. The optical beam paths are indicated by small blue arrowheads, and the T-ray beam paths by the large orange arrowheads.

receiver by an identical set of lenses and mirrors. At the receiver, the initially divided probe beam optically gates the T-ray receiver with a short time duration compared with the arriving T-ray pulse duration. Synchronizing between the optical gating pulse and the T-ray pulse allows the coherent detection of the T-ray signal at a time instance. A complete temporal scan of the T-ray signal is enabled by the discrete micro-motion of a mechanical stage controlling the optical delay line. A sealed dry-air chamber can be used to cover the entire T-ray path to prevent the T-rays from interacting with ambient water vapor, which, otherwise, induces the spectral absorption lines and temporal fluctuations.

3. EFFECTS OF WATER VAPOR ON T-RAY SIGNAL AND SPECTRUM

In order to demonstrate the effects of water vapor on the T-ray signal and spectrum, two chambers with different atmospheres are required, one containing water vapor and the other containing vacuum. However, since such non-polar gas molecules as nitrogen do not demonstrate any T-ray rotational absorption lines, a nitrogen-purged chamber can serve as a replacement to a vacuum chamber, which is mechanically complicated. This also allows accurate measurement of an inherent T-ray signal in comparison with a signal distorted by water vapor.

Figure 2 shows the T-ray signals and spectra measured by THz-TDS under nitrogen and water-vapor atmospheres at room temperature and pressure. The sampling interval is 0.067 ps, corresponding to the sampling frequency of 15 THz. The original time duration is 136 ps, able to resolve the spectral features down to 7.32 GHz. The temporal data is zero-padded prior to FFT, giving an improved frequency resolution of 0.24 GHz.

In the time domain, the signal recorded in the presence of water vapor undergoes long fluctuations after the main pulse. This is due to the energy re-emission by rotational transitions of water molecules. In the frequency domain, the water vapor causes clear absorption lines at discrete frequencies, as a result of quantized rotational transition energy. In terms of Fourier theory, the pair of fluctuations and absorption lines is based on the principle that a sharp feature in one domain is related to a broad feature in the other domain.

Despite the fluctuations and the absorption dips, the analysis shows that the T-ray energy loss by water absorption calculated between 0.0 to 4.0 THz is as high as 10% for the spectrum in Figure 2. The loss is likely to be from the non-directional energy re-emission of the water molecules. In the time domain, the ratio between the main pulse energy to the tail (fluctuation) energy are calculated for both of the time-domain signals (for more details on the calculation, see Section 6.2). The energy ratio for the nitrogen measurement is 429.98, whereas the ratio for the water vapor measurement is 18.82. This difference will be used later on to construct the criterion for fluctuation removal.

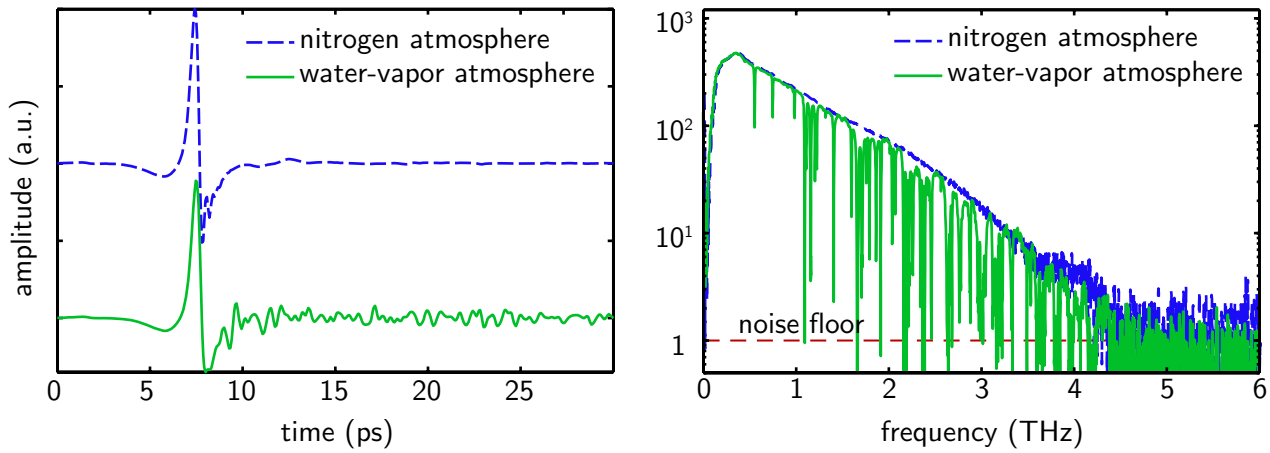

Figure 2. Effects of water vapor on a T-ray pulse and its spectrum. (Left) T-ray pulses recorded under nitrogen and water-vapor atmospheres, and (right) their corresponding spectra. For this measurement the noise floor marks the cutoff frequency at approximately 4.0 THz.

With regard to the system bandwidth, in the figure, the noise floor delimits the cutoff frequency of the system to 4.0 THz. However, the reliable frequency range also depends on the amount of absorption in the sample. Usually, the reliable frequency range is well below the cutoff frequency, because the absorption could easily exceed the dynamic range at high frequencies, where the T-ray energy is inherently low. The T-ray spectrum for water-vapor atmosphere in Figure 2 indicates the reliable frequency range of 1.5 THz.

4. WATER VAPOR AS A BLACK BOX

Given that $x(t)$ denotes the input T-ray pulse, which is just deployed from a transmitter, $s(t)$ the impulse response of a sample, $w(t)$ the impulse response of water vapor, $u(t)$ the impulse response of the system, $n(t)$ the noises, and $r(t)$ the time window, the received pulse $y(t)$ can be described as

$$y(t) \quad = \quad [x(t) * s(t) * w(t) * u(t) + n(t)] \cdot r(t) \; , \tag{1}$$

where $*$ denotes the convolution. This equation is illustrated in Figure 3. In this preliminary study, the noise and the time window are omitted for the sake of simplicity. Thus, the above equation in the frequency domain is

$$Y(\omega) \quad = \quad X(\omega)S(\omega)W(\omega)U(\omega) \; . \tag{2}$$

Here, $Y(\omega)$, $X(\omega)$, $S(\omega)$, $W(\omega)$, and $U(\omega)$ represent complex frequency responses, as the Fourier pairs of $y(t)$, $x(t)$, $s(t)$, $w(t)$, and $u(t)$, respectively.

The water-vapor frequency response can be expressed by

$$W(\omega) \quad = \quad \exp\left[-j\hat{n}_{\text{vap}}\frac{\rho(T)}{\rho_0(T)} \cdot \frac{\omega L}{c}\right] \; . \tag{3}$$

Here, L denotes the T-ray propagation length in free space, excluding the space occupied by sample(s). The water vapor's complex index of refraction $\hat{n}_{\text{vap}} = n_{\text{vap}} - j\kappa_{\text{vap}}$, containing the real index n_{vap} and the extinction coefficient κ_{vap}, is a function of frequency, pressure, and temperature. The water-vapor response is also determined by the humidity,[15] where $\rho(T)$ is the vapor density at temperature T, $\rho_0(T)$ is the saturation vapor density at the same temperature. Equation 3 considers water vapor only and not the gases in the atmosphere such as nitrogen, oxygen, carbon dioxide, etc.

In order to remove the effect of water vapor from a free path, the water-vapor response must be replaced by the vacuum response with the same propagation length, given by

$$V(\omega) \quad = \quad \exp\left[-j\frac{\omega L}{c}\right] \; . \tag{4}$$

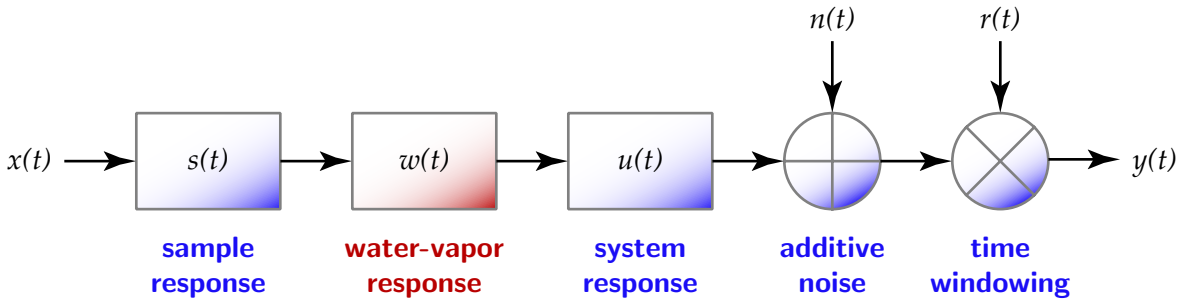

Figure 3. Model of a spectroscopic system. The system comprises impulse responses of sample, water vapor, and system, denoted by $s(t)$, $w(t)$, and $u(t)$, respectively. The signals $x(t)$, $y(t)$, $n(t)$, and $r(t)$ represent input T-ray pulse, measured pulse, noise, and time window, respectively. The water-vapor response is subject to removal.

In such a case, the spectrum of the received pulse, $Y(\omega)$, must be divided by

$$\frac{W(\omega)}{V(\omega)} = \exp\left\{-j\frac{\omega L}{c}\left[\hat{n}_{\text{vap}}\frac{\rho(T)}{\rho_0(T)} - 1\right]\right\} . \tag{5}$$

From the above equation, the required parameters are the T-ray propagation length in free space, L, the water vapor's complex index of refraction, $\hat{n}_{\text{vap}}$, and the vapor densities, $\rho(T)$ and $\rho_0(T)$.

5. SIMULATION OF H_2O ABSORPTION COEFFICIENT AND REFRACTIVE INDEX

The simulation of an absorption coefficient, $\alpha(\omega) = 2\omega\kappa(\omega)/c$, and index of refraction, $n(\omega)$, for an individual rotational transition is based on the Lorentzian line profile,[16]

$$\alpha_a(\omega) = \frac{1}{\pi}\cdot\frac{\Delta\omega_a}{(\omega_a-\omega)^2+\Delta\omega_a^2} , \tag{6a}$$

$$n_a(\omega) = \frac{1}{\pi}\cdot\frac{(\omega_a-\omega)}{(\omega_a-\omega)^2+\Delta\omega_a^2} , \tag{6b}$$

where ω_a denotes a^{th} transition frequency, i.e. the line position, and $\Delta\omega_a$ is the HWHM of the profile. The absorption coefficient and index of refraction are related via Kramers-Kronig relation.

Absorption coefficient and index of refraction, as a result of the absorption line ensemble in the frequencies of interest, are the summation of an offset and a set of Lorentzian line profiles, or

$$\alpha(\omega) = \alpha(0) + \sum_a \alpha_a(\omega) \tag{7a}$$

$$n(\omega) = n(0) + \sum_a n_a(\omega) . \tag{7b}$$

In the simulation the transition frequencies for H_2O molecules are taken from the spectral line catalog reported by Jet Propulsion Laboratory,[17] and the HWHM is 3 GHz, approximately equal for every transition frequency.

Absorption coefficients of water vapor, shown in Figure 4, are determined from measured data (Figure 2) and the Lorentzian model in the frequency range between 0 and 4 THz. It can be clearly seen that below 1.6 THz the model can closely resemble the measurement. This resemblance is possible since the absorption lines in this low frequency range have their strengths beneath the maximum absorption coefficient measurable by the system. However, as the frequency goes beyond 1.6 THz, the maximum measurable absorption coefficient becomes lowered in response to THz-TDS's characteristics, yet some absorption line strengths are larger. In this situation, the system can no longer measure the absorption coefficient correctly, and the clipped absorption peaks are obvious, in particular, in the range from 2 to 4 THz. Furthermore, the quality of the clipped lines is worse, when the T-ray power reaches the noise floor beyond 3 THz.

Given the aforementioned fact, direct deconvolution of the measured response by the water-vapor absorption model cannot remove water-vapor induced fluctuations. In fact, doing so will completely deteriorate the signal.

6. WATER-VAPOR REMOVAL ALGORITHM

From the previous section it has been shown that the measured absorption coefficient is not in accordance with the simulation due to the limiting dynamic range of the system. Thus, this prohibits direct deconvolution of H_2O absorption lines from measured T-ray signals. This section present an iterative algorithm to overcome the problem.

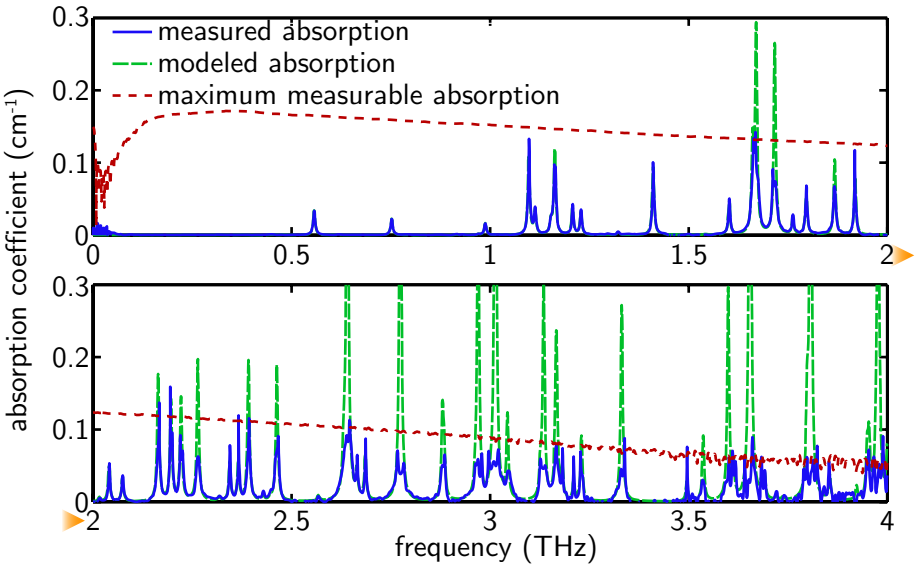

Figure 4. Comparison between measured and modeled absorption coefficients. The measurement can be imitated well by the model in the range of 0.0 to 1.6 THz, but poorly in the higher frequency range, where the absorption strengths become higher than the dynamic range. The maximum measurable absorption coefficient of the system, represented by the dashed line, is calculated using a method of Jepsen and Fischer.[11]

6.1. Fine-tuning of complex absorption lines

The algorithm, shown in Figure 5, starts with fetching H_2O spectral line parameters, including line positions and strengths, in the frequency range of interest from an existing database. The counters a and b for line position and line strength are reset.

A complex absorption line, $n(\omega) - j\kappa(\omega)$, of a rotational transition at $\omega_{a=0}$ is modeled according to Equations 6a and 6b in Section 5. The modeled complex line multiplied by the initial strength factor $m_{b=0}$ is then temporarily deconvolved from the measured fluctuating complex response, $Y(\omega)$. The deconvolved time-domain signal, $y(t)$, is estimated for its fluctuation ratio (see Subsection 6.2). The procedure repeats to find the fluctuation ratio at other predefined line strengths m_b; $b \in \{1, 2, 3, \ldots\}$.

Once the tuning range, m_b, is covered, the algorithm picks up an optimal strength within m_b, which gives the minimum fluctuation ratio, if any, and permanently removes that optimal complex line from the measured signal. The tuning procedure starts again but with the next transition line, $\omega_{a=1}$, and is repeated until all lines are optimized and removed. Since there might be dependence between absorption lines with regard to time-domain fluctuations, the whole process starts again until the fluctuation ratio converges to a minimum.

Note that if the tuning range m_b and its step size are set appropriately, it is not necessary to know the exact values of the propagation length in free air, the temperature, nor the vapor density.

6.2. Fluctuation ratio

A criterion relative to the quality of a T-ray signal is necessary in selecting the optimal absorption line strengths. The 'quality' here is defined as the state of low fluctuations and high pulse energy in the time domain, which implies absence of absorption lines in the frequency domain. In order to determine the quality it must be able to calculate the total energy of the main pulse and of the fluctuations. One potential way is to window the time-domain signal with a Gaussian profile to achieve the amplitude at a desired portion. Figure 6(a) shows a Gaussian window, $g(t)$, overlapping the T-ray pulse, $y(t)$. A Gaussian window with appropriate width and position would eliminate the fluctuating tail, as shown in Figure 6(b). On the other hand, the complement of a Gaussian window could also be used to remove the main pulse, as in Figure 6(c). With the assistance of a

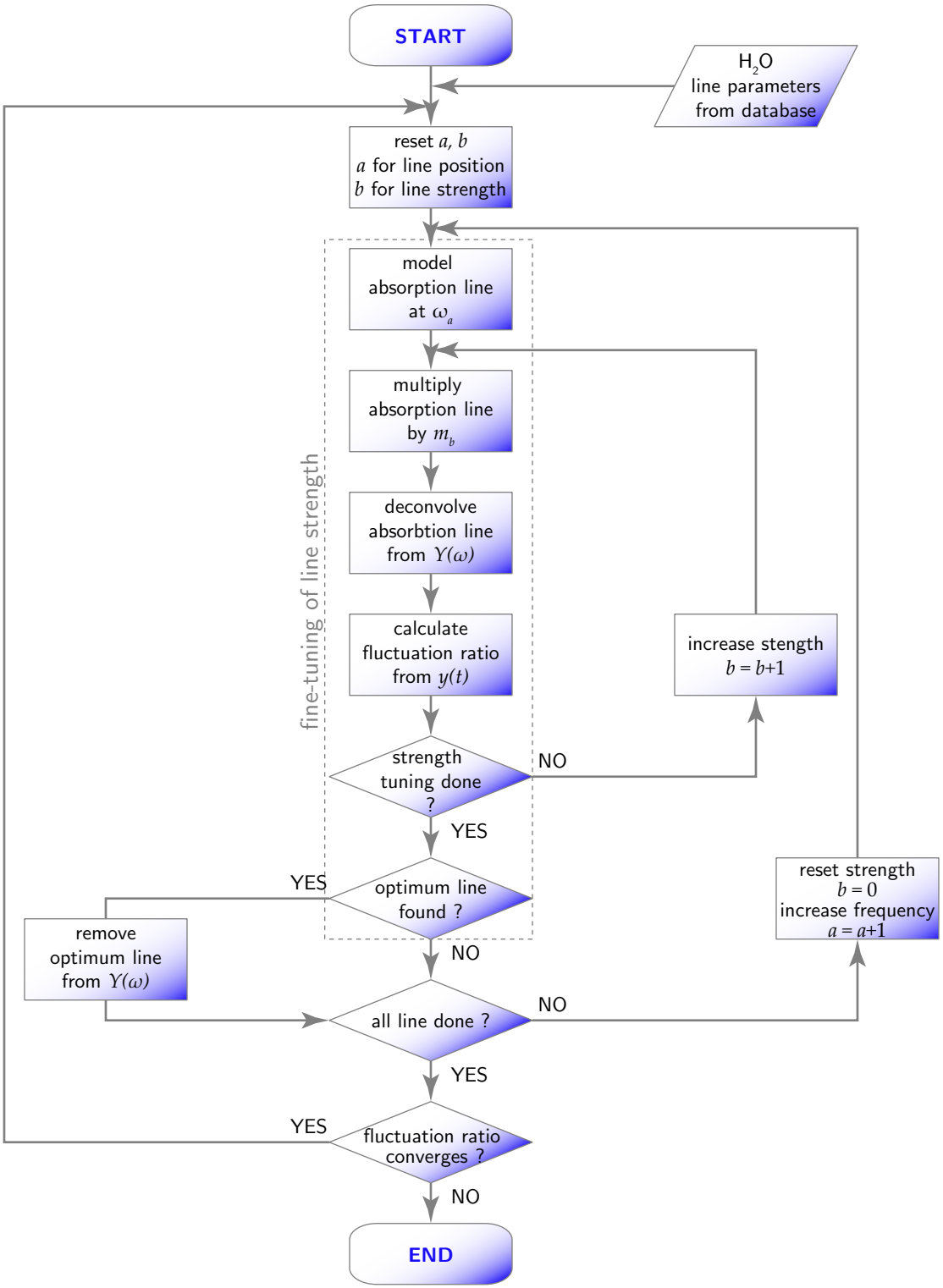

Figure 5. Fluctuation-removal algorithm. Each absorption line in the T-ray frequency range is modeled and fined-tuned in its strength with the criterion of minimum fluctuations, and then the optimal line is removed from the measured complex response. The procedure is repeated until all absorption lines within the frequency range of interest are investigated, and until the fluctuation ratio is no longer decreased.

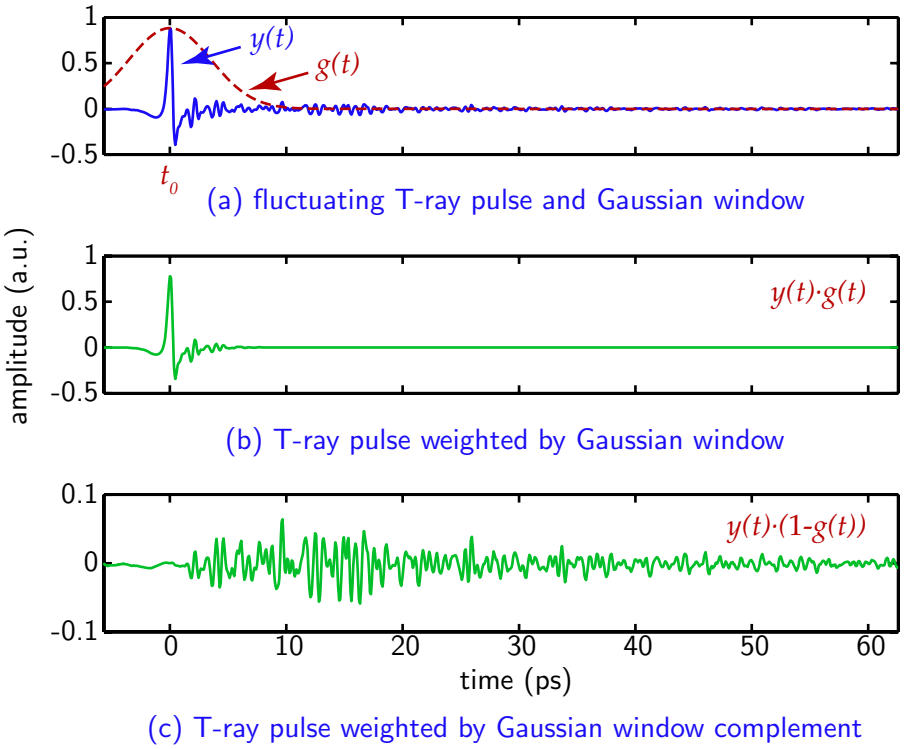

Figure 6. Gaussian window applied to the T-ray signal. A T-ray pulse weighted by a Gaussian window, which has its peak position set exactly at the main pulse peak, yields the main pulse with suppressed fluctuations. A T-ray pulse weighted by the Gaussian window complement yields only fluctuations. The FWHM of the Gaussian window used here is 8.33 ps.

Gaussian window, the main pulse's total energy normalized by the fluctuation energy—coined the fluctuation ratio—can be formulated as

$$F \quad = \quad \frac{\int_t [y(t) \cdot g(t)]^2}{\int_t [y(t) \cdot (1 - g(t))]^2} \, . \tag{8}$$

The integration is carried out over the time duration of a recorded T-ray signal. A Gaussian window is given by

$$g(t) \quad = \quad \exp[-(t - t_0)^2/\sigma^2] \, , \tag{9}$$

where t_0 is the peak position of the T-ray main pulse, and σ multiplied by $2\sqrt{\ln 2}$ is FWHM of a Gaussian window.

6.3. Generality of the algorithm

The algorithm is plausibly general—in the sense that it can be applied to any T-ray signal with minimal disturbance of desired signal features. This generality is due to the fact that: (i) The algorithm alters a T-ray spectrum only at which water-vapor absorption lines are situated. The spectral lines of other polar molecules also occupy a narrow frequency band, and rarely overlap with the water lines. (ii) Any transient feature in the time domain tends to have a corresponding broad feature in the frequency domain. The reflections, for example, which exhibit a fringe pattern over a broad frequency range, are not affected by narrow band absorption line removal.

7. RESULTS

The first T-ray signal, subject to the water-vapor removal algorithm, is measured in free space without the presence of any material. The fine-tuning algorithm is carried out with complex absorption lines in the frequency range between 0.1 and 3 THz, where the T-ray magnitude is relatively high. The FWHM of the Gaussian window is 8.33 ps, the strength factor range, m_b, is from 0 to 2.5 with 200 incremental steps, and the fine-tuning iteration is set to two.

Figure 7 shows the result in comparison with the nitrogen-atmosphere measurement. The algorithm can

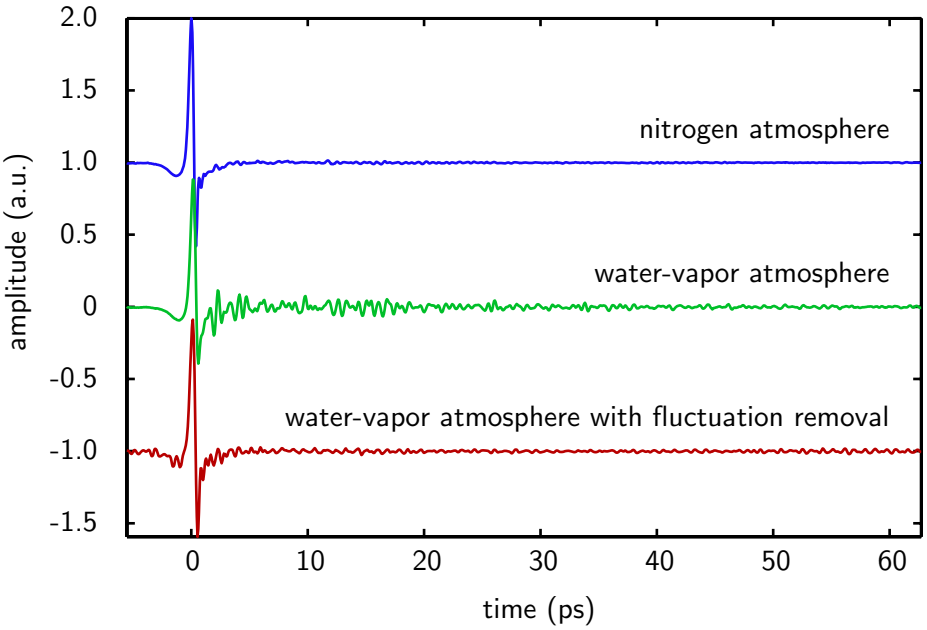

Figure 7. Free space T-ray signals with different atmospheric conditions.

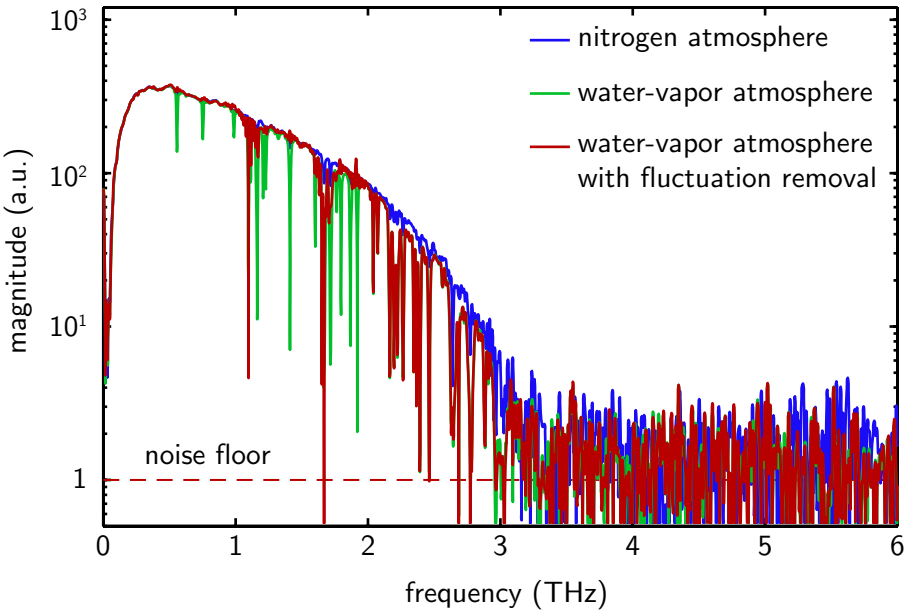

Figure 8. Free space T-ray spectra with different atmospheric conditions.

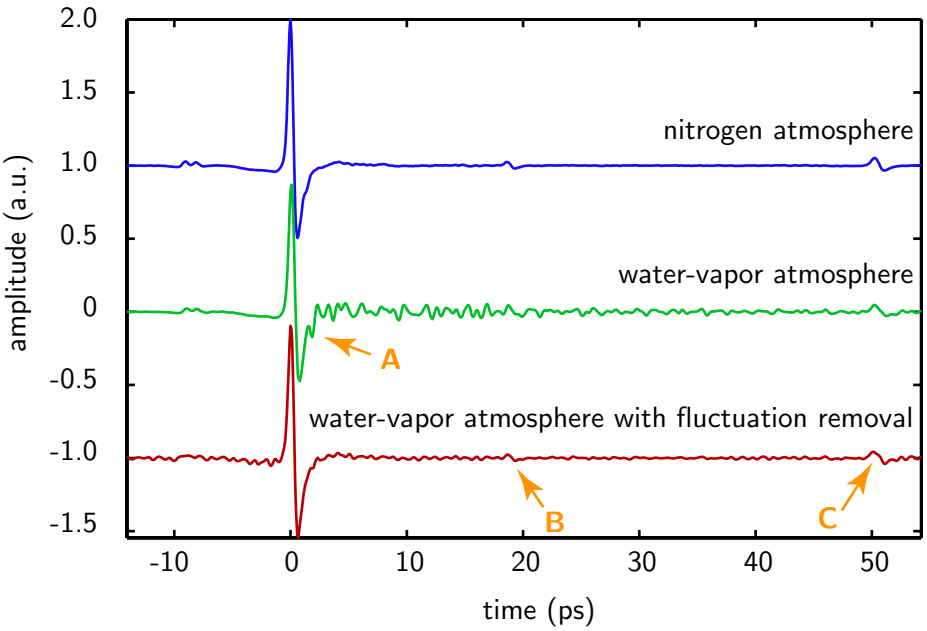

Figure 9. T-ray signals measured with DL-Phenylalanine sample in place. The reflections at 19 and 50 ps are due to the cryostat's windows.

significantly reduce the fluctuations, which are previously located immediately after the main pulse. Despite that, the algorithm itself introduces small fluctuations in front of the main pulse and after 50 ps. The result in the frequency domain, shown in Figure 8, demonstrates the success of the algorithm in removing most of the absorption lines. However, a few lines still persist.

The second tested signal is recorded with a DL-Phenylalanine sample[18] in place at 220 K. The signal contains the reflections, originating from the cryostat's windows, made from Topas. Use of such a signal demonstrates how well the proposed algorithm can deal with water-vapor fluctuations without disturbing unrelated features. The parameters used in the algorithm are similar to the previous test, excepting that the interrogated complex absorption lines are in between 0.1 and 2 THz.

The processed signal is shown in Figure 9. Again, it is obvious that the fluctuations located after the main pulse (point A) are remarkably reduced. The reflection at 50 ps (point C) is not disturbed by the algorithm, and, surprisingly, the reflection at 19 ps (point B), which was initially buried in fluctuations, is now recovered. Figure 10 shows a few absorption lines that cannot be completely removed. These persistent lines are around approximately 1.1 and 1.7 THz, exactly the same position as the unremoved lines in the previous case (see Figure 8). An assumption is that these lines might generate low energy fluctuations, which cannot be tackled by the approach based on the fluctuation ratio measure.

8. CONCLUSION

An algorithm for removal of water-vapor induced fluctuations in T-ray signals is proposed. Theoretically, this could be done by simple deconvolution of the complex water-vapor response, modeled from a spectroscopic catalog, from the measured signal. However, a major factor, which prohibits performing such a simple method, is that the measured rotational absorption lines of water vapor are distorted by the limited dynamic range of the THz-TDS system. A way to circumvent differences between modeled and measured complex responses is to fine-tune the strength of each absorption line. A criterion for tuning of absorption lines is met when the fluctuations reach a minimum. This tuning scheme also relaxes the requirement for precise knowledge of propagation length and ambient atmospheric conditions during measurement.

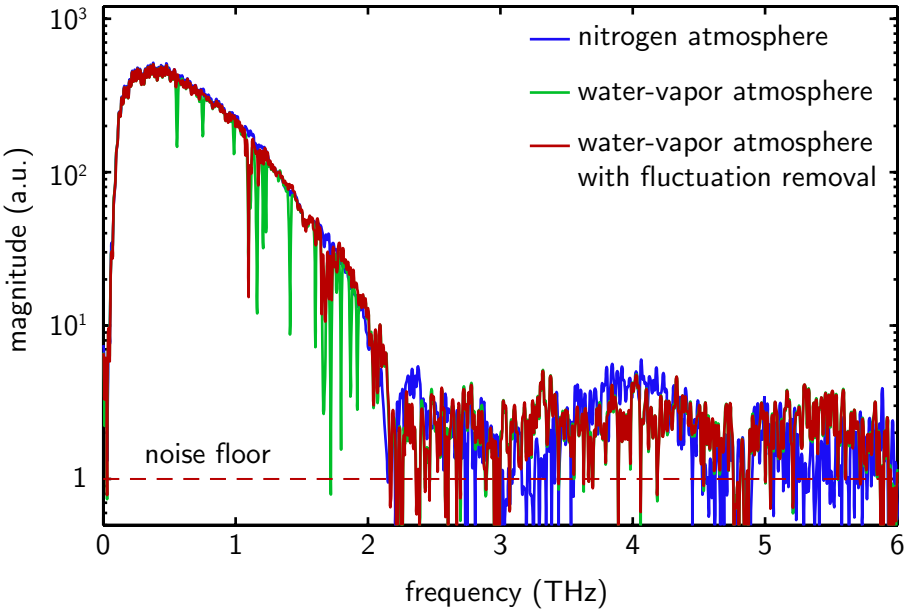

Figure 10. T-ray spectra measured with DL-Phenylalanine sample in place.

The algorithm produces promising results in the way that it can reduce a significant amount of the signal fluctuation with small disturbance to other non-related features, such as reflections. Moreover, the reflections, which are initially masked by fluctuations, can be recovered by the algorithm. However,the preliminary results in the frequency domain show unremoved water-vapor absorption lines. These could probably be due to an unsuitable spectral line profile, unaccounted system's response, sub-optimal Gaussian window, and/or inappropriate line-selection criterion. Work on improvement of the algorithm is ongoing, and also more example signals are being tested to ensure the robustness and generality.

Acknowledgment

The authors would like to thank Morten Franz at the Department of Molecular and Optical Physics, University of Freiburg, for his support in T-ray measurements.

REFERENCES

1. D. M. Mittleman, M. Gupta, R. Neelamani, R. G. Baraniuk, J. V. Rudd, and M. Koch, "Recent advances in terahertz imaging," *Applied Physics B: Lasers and Optics* **68**(6), pp. 1085–1094, 1999.
2. F. Huang, B. Schulkin, H. Altan, J. F. Federici, D. Gary, R. Barat, D. Zimdars, M. Chen, and D. B. Tanner, "Terahertz study of 1,3,5-trinitro-s-triazine by time-domain and Fourier transform infrared spectroscopy," *Applied Physics Letters* **85**(23), pp. 5535–5537, 2004.
3. D. M. Mittleman, R. H. Jacobsen, R. Neelamani, R. G. Baraniuk, and M. C. Nuss, "Gas sensing using terahertz time-domain spectroscopy," *Applied Physics B: Lasers and Optics* **67**(3), pp. 379–390, 1998.
4. B. M. Fischer, M. Hoffmann, H. Helm, G. Modjesch, and P. U. Jepsen, "Chemical recognition in terahertz time-domain spectroscopy and imaging," *Semiconductor Science and Technology* **20**, pp. S246–S253, 2005.
5. L. Thrane, R. H. Jacobsen, P. U. Jepsen, and S. R. Keiding, "THz reflection spectroscopy of liquid water," *Chemical Physics Letters* **240**(4), pp. 330–333, 1995.
6. M. van Exter, C. Fattinger, and D. Grischkowsky, "Terahertz time-domain spectroscopy of water vapor," *Optics Letters* **14**(20), pp. 1128–1130, 1989.
7. D. Grischkowsky, S. Keiding, M. van Exter, and C. Fattinger, "Far-infrared time-domain spectroscopy with terahertz beams of dielectrics and semiconductors," *Journal of the Optical Society of America B: Optical Physics* **7**(10), pp. 2006–2015, 1990.

8. J. F. Federici, B. Schulkin, F. Huang, D. Gary, R. Barat, F. Oliveira, and D. Zimdars, "THz imaging and sensing for security applications–explosives, weapons and drugs," *Semiconductor Science and Technology* **20**, pp. S266–S280, 2005.
9. H.-B. Liu, H. Zhong, N. Karpowicz, Y. Chen, and X.-C. Zhang, "Terahertz spectroscopy and imaging for defense and security applications," *Proceedings of the IEEE* , 2007. (In Press).
10. W. Withayachumnankul, H. Lin, S. P. Mickan, B. M. Fischer, and D. Abbott, "Analysis of measurement uncertainty in THz-TDS," in *Proc. SPIE Microtechnologies for the New Millennium*, **6593**, 2007. Accepted for publication.
11. P. U. Jepsen and B. M. Fischer, "Dynamic range in terahertz time-domain transmission and reflection spectroscopy," *Optics Letters* **30**(1), pp. 29–31, 2005.
12. J. Xu, T. Yuan, S. Mickan, and X. C. Zhang, "Limit of spectral resolution in terahertz time-domain spectroscopy," *Chinese Physics Letters* **20**(8), pp. 1266–1268, 2003.
13. P. Smith, D. H. Auston, and M. C. Nuss, "Subpicosecond photoconducting dipole antennas," *IEEE Journal of Quantum Electronics* **24**(2), pp. 255–260, 1988.
14. L. Xu, X.-C. Zhang, and D. H. Auston, "Terahertz beam generation by femtosecond optical pulses in electro-optic materials," *Applied Physics Letters* **61**(15), pp. 1784–1786, 1992.
15. T. Yuan, H. Liu, J. Xu, F. Al-Douseri, Y. Hu, and X.-C. Zhang, "Terahertz time-domain spectroscopy of atmosphere with different humidity," in *Proc. SPIE Terahertz for Military and Security Applications*, R. J. Hwu and D. L. Woolard, eds., **5070**, pp. 28–37, 2003.
16. C. H. Townes and A. L. Schawlow, *Microwave Spectroscopy*, McGraw-Hill, 1955.
17. H. M. Pickett, R. L. Poynter, E. A. Cohen, M. L. Delitsky, J. C. Pearson, and H. S. P. Müller, "Submillimeter, millimeter, and microwave spectral line catalog," *Journal of Quantitative Spectroscopy and Radiative Transfer* **60**(5), pp. 883–890, 1998.
18. M. Yamaguchi, F. Miyamaru, K. Yamamoto, M. Tani, and M. Hangyo, "Terahertz absorption spectra of L-, D-, and DL-alanine and their application to determination of enantiometric composition," *Applied Physics Letters* **86**(5), art. no. 053903, 2005.